

## RESEARCH ARTICLE

# Skeletal muscle mitochondrial fragmentation and impaired bioenergetics from nutrient overload are prevented by carbon monoxide

 Heath G. Gasier,<sup>1,2</sup> Jacob Dohl,<sup>2</sup> Hagir B. Suliman,<sup>1,4</sup> Claude A. Piantadosi,<sup>1,3,4</sup> and Tianzheng Yu<sup>2</sup>

<sup>1</sup>Department of Anesthesiology, Duke University Medical Center, Durham, North Carolina; <sup>2</sup>Department of Military and Emergency Medicine, Uniformed Services University of the Health Sciences, Bethesda, Maryland; <sup>3</sup>Department of Medicine, Duke University Medical Center, Durham, North Carolina; and <sup>4</sup>Department of Pathology, Duke University Medical Center, Durham, North Carolina

Submitted 9 January 2020; accepted in final form 12 August 2020

**Gasier HG, Dohl J, Suliman HB, Piantadosi CA, Yu T.** Skeletal muscle mitochondrial fragmentation and impaired bioenergetics from nutrient overload are prevented by carbon monoxide. *Am J Physiol Cell Physiol* 319: C746–C756, 2020. First published August 26, 2020; doi:10.1152/ajpcell.00016.2020.—Nutrient excess increases skeletal muscle oxidant production and mitochondrial fragmentation that may result in impaired mitochondrial function, a hallmark of skeletal muscle insulin resistance. This led us to explore whether an endogenous gas molecule, carbon monoxide (CO), which is thought to prevent weight gain and metabolic dysfunction in mice consuming high-fat diets, alters mitochondrial morphology and respiration in C2C12 myoblasts exposed to high glucose (15.6 mM) and high fat (250  $\mu$ M BSA-palmitate) (HGHF). Also, skeletal muscle mitochondrial morphology, distribution, respiration, and energy expenditure were examined in obese resistant (OR) and obese prone (OP) rats that consumed a high-fat and high-sucrose diet for 10 wk with or without intermittent low-dose inhaled CO and/or exercise training. In cells exposed to HGHF, superoxide production, mitochondrial membrane potential ( $\Delta\Psi_m$ ), mitochondrial fission regulatory protein dynamin-related protein 1 (Drp1) and mitochondrial fragmentation increased, while mitochondrial respiratory capacity was reduced. CO decreased HGHF-induced superoxide production, Drp1 protein levels and mitochondrial fragmentation, maintained  $\Delta\Psi_m$ , and increased mitochondrial respiratory capacity. In comparison with lean OR rats, OP rats had smaller skeletal muscle mitochondria that contained disorganized cristae, a normal mitochondrial distribution, but reduced citrate synthase protein expression, normal respiratory responses, and a lower energy expenditure. The combination of inhaled CO and exercise produced the greatest effect on mitochondrial morphology, increasing ADP-stimulated respiration in the presence of pyruvate, and preventing a decline in resting energy expenditure. These data support a therapeutic role for CO and exercise in preserving mitochondrial morphology and respiration during metabolic overload.

fission; fusion; mitochondria; obesity; respiration

## INTRODUCTION

Mitochondrial dynamics, defined by mitochondrial movement along the cytoskeleton, tethering, and shape changes through fusion and fission, are involved in cellular ATP provision (2, 25, 58). Fusion occurs when the inner and outer mitochondrial membranes of two mitochondria fuse in separate steps, with the inner regulated by optic atrophy gene 1 (OPA1) and outer by mitofusion 1 and 2 (Mfn 1 and 2) (34). Fission is

mediated by dynamin-related protein 1 (Drp1) and fission 1 homolog protein (Fis1) (46, 54). Fused mitochondria elongate and possess a higher capacity, and likely higher efficiency, to synthesize ATP, and are safe from mitophagy (20, 31, 51). Mitochondria that have undergone fission are smaller with a fragmented appearance, a reduced mitochondrial membrane potential ( $\Delta\Psi_m$ ) due to uncoupling of respiration or damage, and undergo mitophagy if membrane potential is not restored (31, 51). Indeed, increased nutrient delivery without a corresponding demand shifts mitochondrial dynamics toward fission, causing fragmentation, increased oxidant production, and a reduced respiratory capacity, promoting obesity and predisposing to type 2 diabetes (3, 15, 38, 55).

Obesity is a component of metabolic syndrome, which also encompasses type 2 diabetes, hypertension, and cardiovascular disease, and exacerbates cancer and many other diseases (9). The prevalence of obesity and type 2 diabetes is rising in the US, and by 2030, projections point to 65 million more obese adults and up to 8.5 million newly diagnosed type 2 diabetics (52). Hence, all avenues for obesity prevention and treatment are critically important to medical practice.

One new strategy that has led experimentally to a reduction in adiposity and prevention of metabolic dysfunction in mice consuming high-fat diets is the use of carbon monoxide (CO) (6, 26, 27, 57), an endogenous gas molecule generated by heme catabolism (49). CO selectively binds to iron centers contained within heme proteins, such as hemoglobin, myoglobin, and cytochrome *c* oxidase, the terminal enzyme of the mitochondrial electron transport chain (12). CO binding to heme *a*<sub>3</sub> of cytochrome *c* oxidase reduces enzyme activity and increases cytochrome *bc*<sub>1</sub> complex reduction (7, 8, 47, 59). The electron accumulation and increased oxygen availability at complex III stimulate mitochondrial superoxide ( $O_2^{\cdot-}$ ); hence, its conversion to hydrogen peroxide ( $H_2O_2$ ), e.g., via superoxide dismutase (47, 56, 59). An antiobesity effect of CO may be due to the increased  $H_2O_2$  that acts as a signal to stimulate mitochondrial biogenesis in the liver, lung, heart, and skeletal muscle, leading to an increase in respiratory capacity (16, 41, 44, 47). Alternatively, CO may increase the expression of uncoupling protein 1 in adipose tissue that is accompanied by an increase in energy expenditure (27). Uncoupling respiration has long been considered an attractive idea for treating obesity and metabolic disease (23, 48), but this compromises ATP production may cause hyperthermia.

Correspondence: H. G. Gasier (heath.gasier@duke.edu).

The effects of CO on skeletal muscle mitochondria during periods of excess nutrient availability remain unknown. Our goal was to test the hypothesis that CO delivered via carbon monoxide-releasing molecule 3 (CORM-3) increases respiratory capacity and prevents mitochondrial fission and fragmentation in C2C12 mouse myoblasts exposed to hyperglycemia and hyperlipidemia. C2C12 myoblasts were selected because they were previously used to establish a model for studying diabetic conditions *in vitro* (15). In addition, we measured skeletal muscle mitochondrial morphology, respiration, and energy expenditure in a study undertaken to measure the reported antiobesity potential of intermittent low-dose inhaled CO in rats (19).

## MATERIALS AND METHODS

**Cell culture experimental protocol.** C2C12 mouse myoblasts (ATCC CRL-1772) acclimated to low-glucose (LG; 5.6 mM) Dulbecco's modified Eagle's medium (DMEM) supplemented with 10% fetal bovine serum (FBS), 100 units/ml penicillin, and 100  $\mu\text{g}/\text{mL}$  streptomycin were cultured in a humidified incubator with 5%  $\text{CO}_2$  at 37°C. Cells were passaged every 2–3 days to maintain confluency <60% and prevent differentiation. On the day of the experiments, myoblasts were treated with 20  $\mu\text{M}$  of CORM-3 (MilliporeSigma, St. Louis, MO) or an equal volume of dimethyl sulfoxide (DMSO, control) and incubated at 37°C in 5%  $\text{CO}_2$  for 30 min. We selected a 20- $\mu\text{M}$  treatment dose of CORM-3 based on published work (32), and our preliminary experiments that showed mitochondrial toxicity at doses >30  $\mu\text{M}$ . CORM-3 is a ruthenium-based compound with a

half-life of 1 min (11). The medium was then changed to either LG DMEM (5.6 mM) with 0.17 mM BSA or high-glucose (15.6 mM) and high-fat (BSA-conjugated palmitate, 250  $\mu\text{M}$ ) DMEM (HGHF), as described previously (15) and supplemented with 1 mM of L-carnitine hydrochloride and 100 nM insulin. CORM-3 (20  $\mu\text{M}$ ) or DMSO was added to the respective dishes, and incubated at 37°C in 5%  $\text{CO}_2$  for 4 h. In total, four groups were studied: LG, LG + CORM-3, HGHF, and HGHF + CORM-3. Protocol modifications were made for respiration experiments (below).

***In vivo rat protocol.*** We had previously determined the effects of low-dose inhaled CO, with and without moderate aerobic exercise, on obesity prevention in male obese resistant CD (OR;  $n = 14$ ) and obese prone CD (OP;  $n = 48$ ) rats aged 8 wk old (Charles River, Germantown, MD) (19). All study procedures were approved by the Uniformed Services University of the Health Sciences (USUHS) Institutional Animal Care and Use Committee. In brief, the animals were housed (2 per cage) in a climate-controlled animal facility with a reverse 12:12-h light-dark cycle. OP rats were assigned by body mass to OP ( $n = 14$ ), OP and carbon monoxide (OP + CO,  $n = 14$ ), OP and exercise (OP + EX,  $n = 10$ ), and OP and carbon monoxide and exercise (OP + COEX,  $n = 10$ ). For 10 wk, the OP rats consumed a high-fat and high-sucrose diet (42% fat and 43% carbohydrate; 4.5 kcal/g), whereas OR rats consumed a low-fat control diet (13% fat and 68% carbohydrate 3.6 kcal/g). Diets were prepared by Teklad Custom (Harlan Laboratories, Madison, WI), and animals had access to food and water *ad libitum*. The CO treatments consisted of 1-h exposures at 250 ppm (5 treatments before and 2 treatments per week during the experiment). Exercise training consisted of forced treadmill running 3 h per week on a rodent treadmill with electrical stimulus (Exer 3/6,

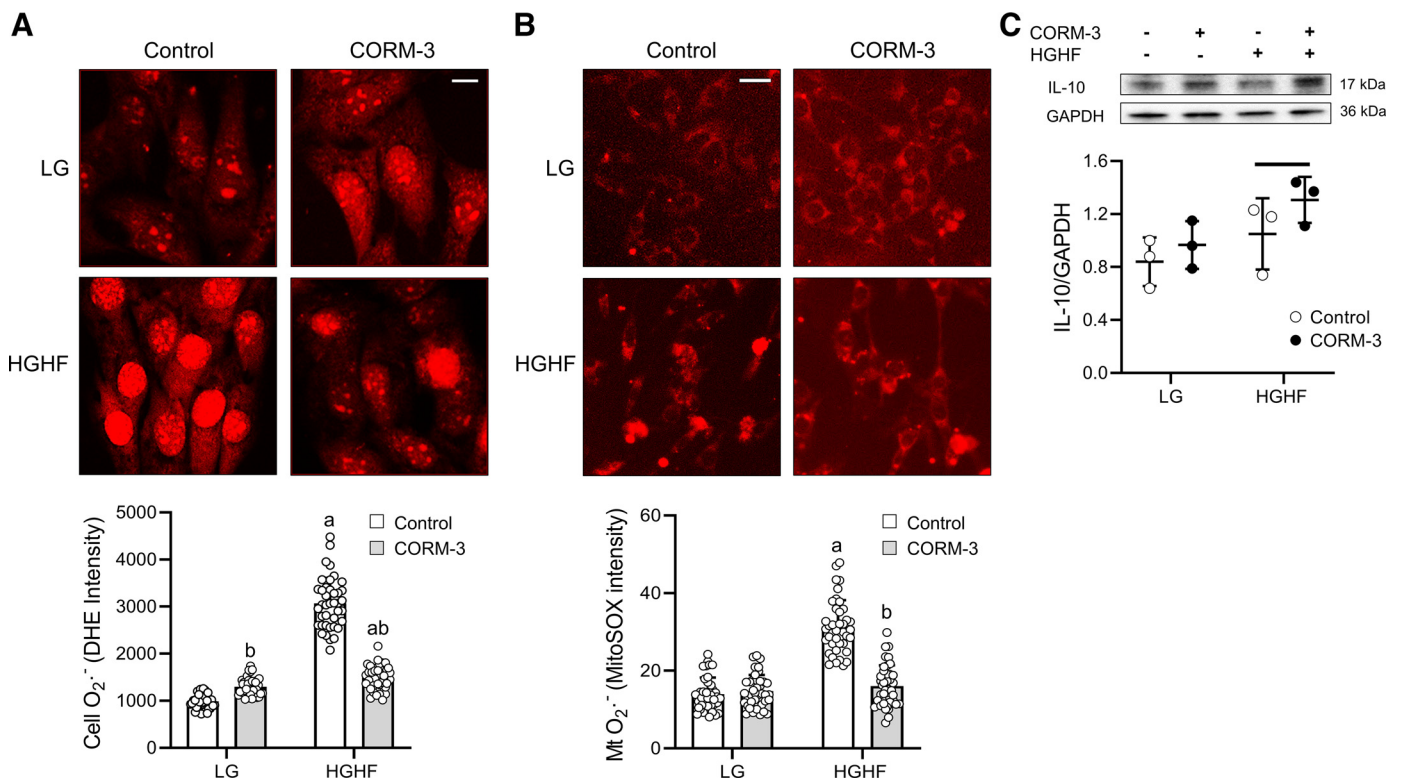


Fig. 1. The high-glucose and high-fat (HGHF)-induced increase in  $\text{O}_2^{\cdot -}$  production is reduced in C2C12 cells treated with carbon monoxide-releasing molecule 3 (CORM-3). Cells were incubated in low glucose (LG) or HGHF and treated with DMSO or CORM-3 for 4 h. **A** and **B**: representative fluorescent images ( $\times 10$  magnification; scale bar = 10  $\mu\text{m}$ ) of cells labeled with DHE and MitoSOX Red. Levels of  $\text{O}_2^{\cdot -}$  were measured by quantifying the fluorescence intensity of ethidium (cellular) and MitoSOX Red (mitochondria) in 40 cells per group. **C**: representative immunoblots and densitometry of interleukin 10 (IL-10) normalized to glyceraldehyde 3-phosphate dehydrogenase (GAPDH). Data were analyzed using a two-way ANOVA with Holm-Sidak test and are presented as individual data points from 1 of 3 independent experiments with means  $\pm$  SD bars. Significant main effect of condition, and condition  $\times$  treatment: line = condition ( $P < 0.05$ ); <sup>a</sup>condition within treatment and <sup>b</sup>treatment within condition ( $P < 0.001$ ).

Columbus Instruments, Columbus, OH) at a grade of 10°, starting at 20 m/min and increasing by 1 m/min to a maximum of 25 m/min that was achieved by the end of week 6. After 10 wk, resting  $\dot{V}O_2$  and  $\dot{V}CO_2$ , respiratory exchange ratio (RER), and energy expenditure were measured and calculated using open circuit calorimetry (Oxymax-Comprehensive Laboratory Animal Monitoring System, Columbus Instruments, Columbus, OH). Each test was performed between 7:00 AM and 12:00 PM, and the rats were restrained within the metabolic chamber and allowed to rest for 5 min before testing. Measurements were collected every 30 s for 20 min, and the airflow rate was maintained at 2–3 L/min. Forty-eight hours before euthanasia and muscle harvest, a run to exhaustion test was performed in OP + EX and OP + COEX rats.

**Mitochondrial mass and morphology,  $\Delta\Psi_m$ ,  $O_2^-$ , and lipids in C2C12 myoblasts.** Mitochondrial mass and morphology were measured after the uptake of 100 nM Mitotracker Red CMXRos by the cells.  $\Delta\Psi_m$  was measured with 100 nM tetramethylrhodamine ethyl ester (TMRE). Cellular and mitochondrial  $O_2^-$  levels were measured with 5  $\mu$ M of dihydroethidium (DHE) and MitoSOX Red, respectively. Intramyocellular lipid content was determined with 2 mg/mL of Nile red. Fluorescent dyes were purchased from ThermoFisher Scientific (Waltham, MA) and added 15 (Mitotracker Red CMXRos and TMRE) or 30 (DHE, MitoSOX Red and Nile red) min before imaging with a Nikon Ti-E epifluorescence microscope (Nikon, Tokyo, Japan) and sCMOS pco.edge 4.2 digital camera (PCO AG, Kelheim, Germany). Excitation/emission wavelengths were 555/613 nm. Images were analyzed using ImageJ software (NIH, Bethesda, MD). For mitochondrial mass, the fluorescence intensity per unit area was measured in 40 cells obtained from 4 sections/group (14, 22). For mitochondrial morphology, ~650 cells were analyzed from 4 to 6 sections/group, and the percentage of cells with fragmented or tubular/elongated mitochondria was determined. We define mitochondrial

fragmentation as the mitochondrial population in cells appearing predominantly as small puncta, lacking in a tubular and interconnected network (15).

**Mitochondrial respiration and extracellular acidification rate measurements in C2C12 myoblasts.** Cells in LG DMEM were seeded in Seahorse 96-well plates (Agilent Technologies, Santa Clara, CA) at a density of  $1.2 \times 10^4$ , total volume 200  $\mu$ L/well, and incubated at 37°C in 5%  $CO_2$  for 72 h. On experimentation days, cells were pre-treated with 20  $\mu$ M CORM-3, or inactive CORM-3 (i-CORM3) for 30 min. iCORM-3 was made in phosphate-buffered saline (PBS, pH 7.4) exposed to room air for 48 h. Two timed experiments were performed to determine the effects of CORM-3 on respiratory control in cells exposed to HGHF. In *experiment 1*, the medium was changed to LG (5.6 mM) and the cells were treated with either CORM-3 or iCORM-3 and incubated at 37°C in 5%  $CO_2$  for 4 h. After incubation, the plate was washed two times with Seahorse XF base medium supplemented with 5.6 mM glucose, 1 mM sodium pyruvate, and 4 mM glutamine (pH 7.4). Fresh media supplemented with 17 mM BSA (pH 7.4) was added to the wells and incubated at 37°C in 0%  $CO_2$  for 1 h. For a Mito Stress Test on a Seahorse XFe96 Analyzer (Agilent Technologies), 45  $\mu$ L of media containing an additional 10 mM glucose, 250  $\mu$ M of BSA-palmitate, 1 mM L-carnitine hydrochloride, and 100 nM insulin (pH 7.4) were added to the wells for a final volume of 180  $\mu$ L. In *experiment 2*, 180  $\mu$ L of either LG (5.6 mM) or HGHF (15.6 mM, 250  $\mu$ M) supplemented with 1 mM L-carnitine hydrochloride and 100 nM insulin were added to the wells with either CORM-3 or iCORM-3. The plate was incubated at 37°C in 5%  $CO_2$  for 4 h and washed two times with Seahorse XF base medium supplemented with 5.6 mM glucose, 1 mM sodium pyruvate, and 4 mM glutamine (pH 7.4) and incubated in the same media at 37°C in 0%  $CO_2$  for 1 h before the Mito Stress Test. Proton leak was determined by adding 2  $\mu$ M oligomycin (ATP synthase inhibitor), maximal uncoupled respiration

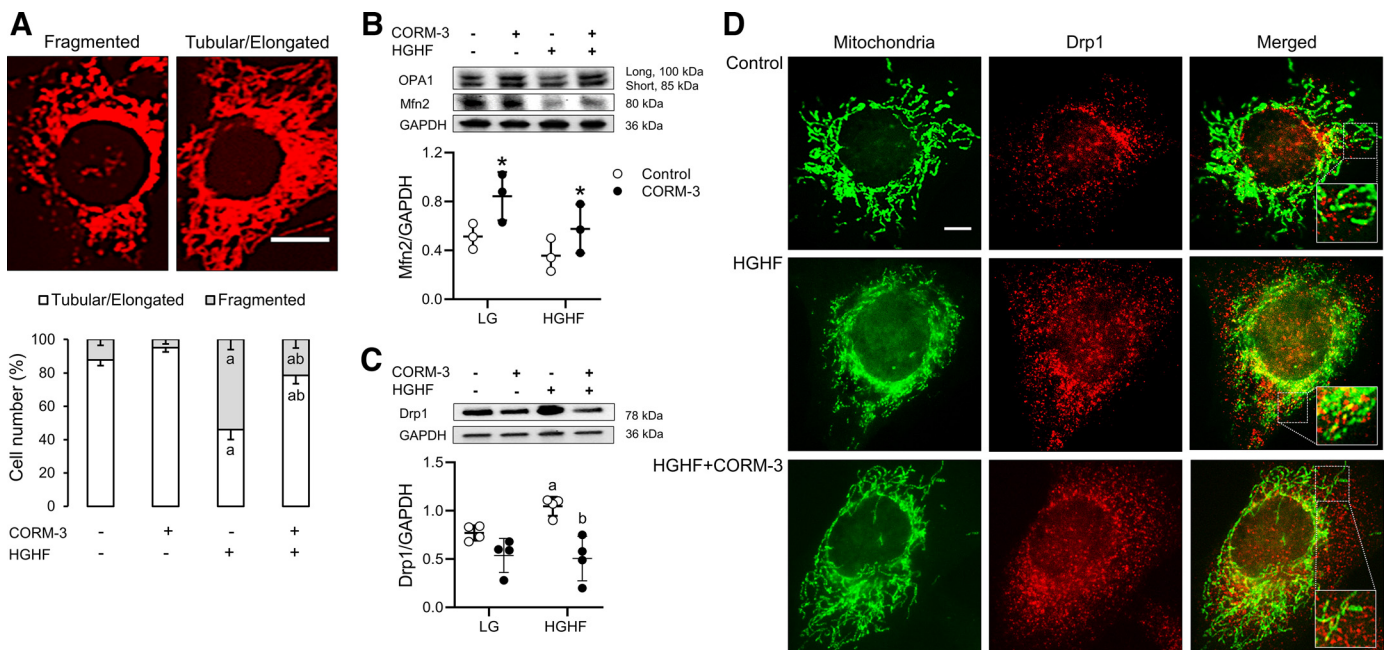


Fig. 2. Carbon monoxide-releasing molecule 3 (CORM-3) attenuates high-glucose and high-fat (HGHF)-induced mitochondrial fragmentation in C2C12 cells. Cells were incubated in low glucose (LG) or HGHF and treated with DMSO or CORM-3 for 4 h. **A**: representative fluorescent images ( $\times 20$  magnification; scale bar = 10  $\mu$ m) of cells labeled with MitoTracker Red CMXRos. The percentage of cells with tubular/elongated and fragmented mitochondria was determined in ~650 cells from 4 to 6 sections/group. Data are presented as means  $\pm$  SD of 3 independent experiments. **B** and **C**: representative immunoblots of optic atrophy type 1 (OPA1), mitofusion 2 (Mfn2), and dynamin-related protein 1 (Drp1). Densitometry of Mfn2 and Drp1 is normalized to GAPDH. Data were analyzed using a two-way ANOVA with Holm-Sidak test and are presented as individual data points from 3 to 4 independent experiments with means  $\pm$  SD bars. Significant main effect of treatment, and condition  $\times$  treatment: \*treatment ( $P < 0.05$ ); <sup>a</sup>condition within treatment and <sup>b</sup>treatment within condition ( $P < 0.001$ ). **D**: representative fluorescent microscopy images ( $\times 40$  magnification; scale bar = 5  $\mu$ m) of cells labeled with cytochrome *c* (green), Drp1 (red), and merged. Drp1 colocalized in puncta of fragmented mitochondria (HGHF, middle row) but not control (top row) or HGHF + CORM-3 (bottom row).

was determined by adding 2  $\mu\text{M}$  carbonyl cyanide *p*-trifluoromethoxyphenylhydrazone (FCCP; uncoupler), and nonmitochondrial respiration was determined by adding 1  $\mu\text{M}$  rotenone (complex I inhibitor) and antimycin A (complex III inhibitor). Nonmitochondrial respiration and ATP-linked respiration were calculated by standard procedures (5). Extracellular acidification rates (ECAR) were used as an indicator of glycolysis. ECAR values obtained after the addition of oligomycin represented an estimate of maximal glycolysis. Immediately after the experiments, the plates were washed with 50  $\mu\text{L}$  of warmed PBS two times before adding 25  $\mu\text{L}$  of ice-cold PBS and shaking for 5 min. The mean protein concentration in LG- and HGHF-treated cells were  $5.5 \pm 1.1$  (SD) and  $6.8 \pm 1.0$   $\mu\text{g}/\text{mL}$ , respectively, and were not statistically different.

**Mitochondrial respiration in permeabilized muscle fibers.** Immediately upon euthanasia, the left soleus muscle was excised and placed in ice-cold relaxing medium (BIOPS) that contained the following (in mM): 2.77  $\text{CaK}_2\text{EGTA}$ , 7.23  $\text{K}_2\text{EGTA}$ , 15 phosphocreatine, 5.77 ATP, 6.56  $\text{MgCl}_2 \cdot 6\text{H}_2\text{O}$ , 20 taurine, 20 imidazole, 0.5 dithiothreitol, and 50 4-morpholineethanesulfonic acid hydrate. The soleus muscle was dissected in ice-cold BIOPS using a stereomicroscope and forceps. Fiber bundles were permeabilized with saponin (50  $\mu\text{g}/\text{mL}$ ) added to BIOPS and rotated for 30 min at 4°C. The fibers were then washed in MIR05 solution (0.5 mM EGTA, 3 mM  $\text{MgCl}_2 \cdot 6\text{H}_2\text{O}$ , 60 mM K-lactobionate, 20 mM taurine, 10 mM  $\text{KH}_2\text{PO}_4$ , 20 mM HEPES, 110 mM sucrose, and 1 g/L fatty acid free BSA) for 10 min

(3 times) at 4°C under gentle rotation. Fibers were then transferred to 1-mL chambers (MS200A Respirometry System, Strathkelvin Instruments Limited, North Lanarkshire, SCO) containing MIR05 with 20 mM creatine monohydrate and 25  $\mu\text{M}$  blebbistatin (42). Complex I leak respiration ( $\text{CI}_L$ ) and state 3 maximal respiration were determined by adding 5 mM malate + 10 mM sodium pyruvate and 5 mM ADP, respectively. Oligomycin (10  $\mu\text{g}$ ) was added to determine the leak control ratio (state 4o/state 3), an indicator of coupling efficiency. Maximal fatty acid oxidative capacity was determined by adding 50  $\mu\text{M}$  palmitoyl L-carnitine chloride + 5 mM ADP. Cytochrome *c* (10  $\mu\text{M}$ ) was added to ensure intactness of the outer mitochondrial membrane, i.e., > 10% were excluded. The mean of two samples per animal was used for data analysis and normalized to muscle wet weight.

**Immunoblotting.** Protein from cell lysate (10  $\mu\text{g}$ ) or soleus muscle homogenate (10–20  $\mu\text{g}$ ) was separated by polyacrylamide gel electrophoresis, and immunoblotting was performed to determine protein expression. Antibodies were purchased from Cell Signaling Technology (Danvers, MA) unless otherwise stated: IL-10 (12163S), citrate synthase (14309S), peroxisome proliferator-activated receptor  $\gamma$ -coactivator 1 $\alpha$  (PGC-1 $\alpha$ ; 2178S; C2C12 cells), PGC-1 $\alpha$  (ab54481, Abcam, Cambridge, MA; tissue), mitochondrial transcription factor A (TFAM; 7395S), subunits of mitochondrial complexes I–V (total OXPHOS; MS604-300, Abcam), mitofusion 2 (Mfn2; 9482S; C2C12 cells), Mfn2 (sc-100560, Santa Cruz Biotechnology, Dallas, TX;

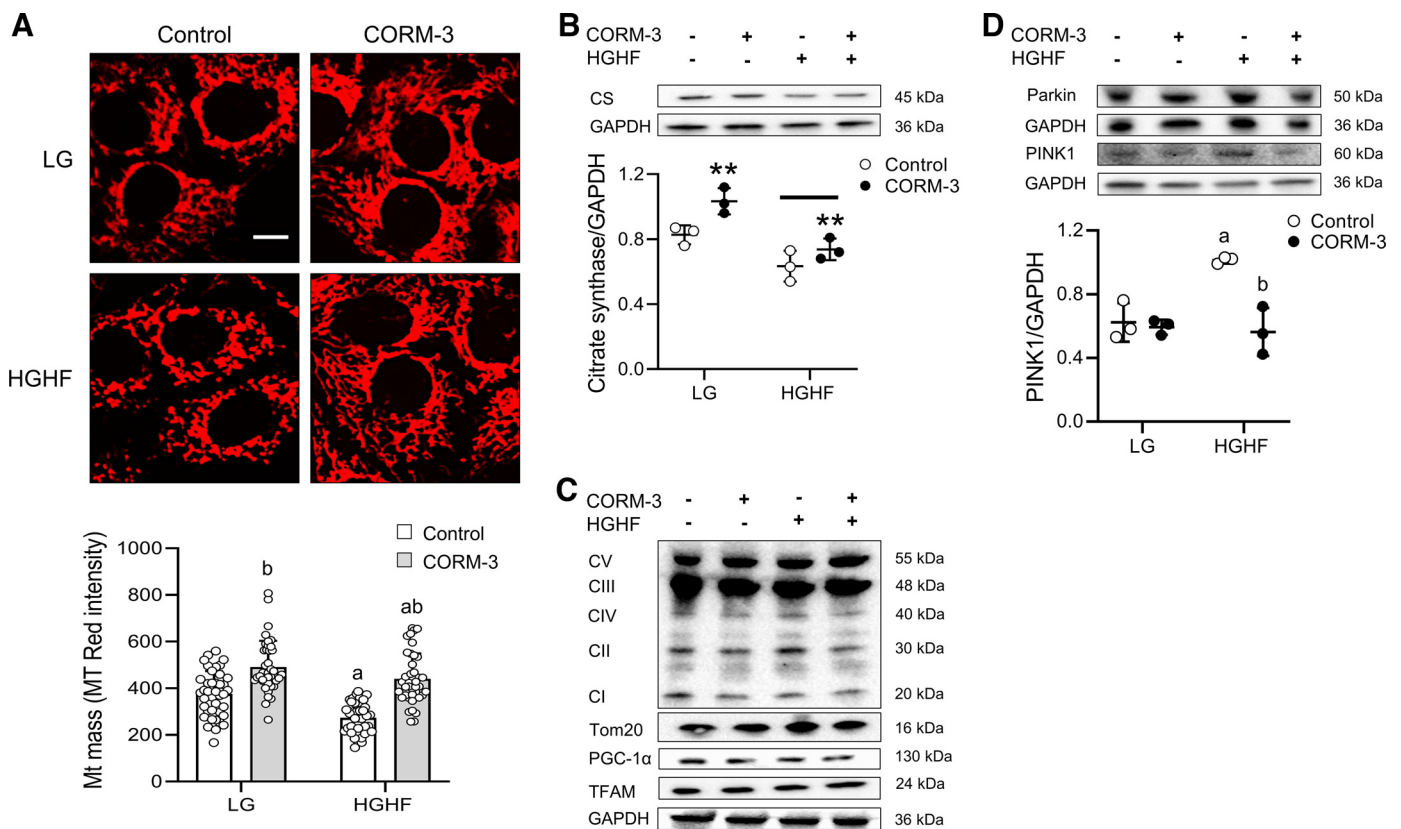


**Fig. 3.** Carbon monoxide-releasing molecule 3 (CORM-3) increases mitochondrial (Mt) mass and represses induction of phosphatase and tensin homolog-induced kinase 1 (PINK1)-mediated mitophagy in C2C12 cells. Cells were incubated in low glucose (LG) or in high glucose and high fat (HGHF) and treated with DMSO or CORM-3 for 4 h. **A:** representative fluorescent images ( $\times 20$  magnification; scale bar = 10  $\mu\text{m}$ ) of cells labeled with MitoTracker Red CMXRos. Mitochondrial mass was measured by quantifying the fluorescence intensity of MitoTracker Red per unit area in 40 cells from 4 sections/group. **B:** representative immunoblots and densitometry of citrate synthase (CS) normalized to GAPDH. **C:** representative immunoblots of mitochondrial complexes I–V subunits, peroxisome proliferator-activated receptor  $\gamma$ -coactivator 1 $\alpha$  (PGC-1 $\alpha$ ), mitochondrial transcription factor A (TFAM), translocase of outer membrane (TOM20), and GAPDH. Densitometry is not shown (nonsignificant). **D:** representative immunoblots of parkin and PINK1. Densitometry shown only for PINK1 normalized to GAPDH. Data were analyzed using a two-way ANOVA with Holm Sidak test and are presented as individual data points from 3 independent experiments with means  $\pm$  SD bars. Significant main effect of condition, treatment, and condition  $\times$  treatment: line = condition ( $P < 0.001$ ); \*\*treatment ( $P < 0.01$ ); <sup>a</sup>condition within treatment and <sup>b</sup>treatment within condition ( $P < 0.001$ ).

tissue), optic atrophy 1 (OPA1; 80471S), dynamin-related protein 1 (Drp1; 5391S), phosphatase and tensin homolog-induced kinase 1 (PINK1; 6946S), parkin (4211S), AMP-activated protein kinase- $\alpha$  (AMPK $\alpha$ ; 2532S), phospho-AMPK $\alpha$  (Thr 172; 2531S), glyceraldehyde 3-phosphate dehydrogenase (GAPDH; ABS16, Millipore-Sigma, Burlington, MA), and translocase of outer membrane (TOM20; 42406S). All antibodies were diluted 1:1,000 except for GAPDH and TOM20, 1:5,000. Secondary antibodies included horseradish peroxidase-conjugated anti-rabbit and anti-mouse (1:10,000). PVDF membranes were developed with enhanced chemiluminescence, and proteins quantified by densitometry (ImageJ) and expressed relative to GAPDH, TOM20, or total protein (Coomassie stain).

**Immunofluorescence.** C2C12 myoblasts were cultured on coverslips (30–40% confluency), fixed with 4% paraformaldehyde, and permeabilized using 0.1% Triton X-100. Cells were incubated with mouse anti-cytochrome (Cell Signaling) and rabbit anti-Drp1 (1:1,000) at 37°C for 1 h, washed in PBS three times, and incubated with anti-mouse Alexa Fluor 488 and anti-rabbit Alexa Fluor 594 (ThermoFisher Scientific) at room temperature for 1 h. Fluorescence images were adjusted using ImageJ.

**Transmission electron microscopy.** In a subset of rats ( $n = 3$ /group) following isoflurane euthanasia, whole body perfusion was performed by left ventricular infusion of 50 ml of fixative comprised of 2% formaldehyde and 2% EM grade glutaraldehyde (Electron Microscopy Sciences, Hatfield, PA) in 0.1 M cacodylate buffer (pH 7.2). Soleus muscle cross-sectional cuts were made to obtain ~1-mm<sup>3</sup> pieces that were placed in the same fixative and stored at 4° for 24 h. The samples were washed three times for 5 min in cacodylate buffer without aldehydes and then incubated in 2% OsO<sub>4</sub> in 0.1 M cacodylate buffer (pH 7.2) for 1 h and washed three times for 10 min in cacodylate buffer. Samples were sent to the USUHS Biomedical Instrumentation Center for preparation. Imaging was completed using a JEOL JEM-1011 transmission electron microscope (JEOL, Peabody, MA). Images collected at  $\times 12$ – $15,000$  magnification were used to determine mitochondrial number and the following morphological parameters (45): surface area, length, perimeter, circularity, Feret's diameter (longest distance between any 2 points), form factor (perim-

eter/ $4\pi \times$  surface area, measure of complexity and branching aspect of mitochondria), and aspect ratio (length to width ratio). Only intermyofibrillar mitochondria (~400/animal) with well-defined borders were traced and analyzed using ImageJ.

**Statistical analysis.** Data were analyzed using SigmaPlot version 14.0 (Systat Software, San Jose, CA) and SPSS Statistics 26.0 (IBM Corp., Armonk, NY). A two-way ANOVA was used to compare condition (HGHF vs. LG), treatment (CORM vs. control), and the interaction (condition  $\times$  treatment) in C2C12 cells. The data were transformed if the variances were unequal (Brown-Forsythe). A one-way ANOVA was used to compare mean group differences for indirect calorimetry with a Holm-Sidak post hoc test. A Kruskal-Wallis one-way ANOVA with Tukey or Dunn's post hoc test was used to compare mean group differences for permeabilized muscle fiber respiration and transmission electron microscopy data, respectively. A *t* test was used to compare the effect of CORM-3 treatment with control on respiration in C2C12 cells acutely exposed to HGHF and to compare the effect of inhaled CO with control on running performance in rats. When the data were not normally distributed, a Mann-Whitney Rank Sum test was performed. Effect sizes (Cohen's *d*) were calculated for transmission electron microscopy and exhaustive exercise tests. For consistency, data are presented as means  $\pm$  SD and medians with quartiles and stated in the figure legends.  $P < 0.05$  was considered statistically significant.

## RESULTS

**CORM-3 and HGHF-induced O<sub>2</sub><sup>-</sup> production in C2C12 cells.** Cellular and mitochondrial O<sub>2</sub><sup>-</sup> production was 3.1- and 2.2-fold higher in HGHF cells, respectively (Fig. 1, A and B). In LG cells, CORM-3 led to a modest increase in cellular but not mitochondrial O<sub>2</sub><sup>-</sup> production. In HGHF cells, CORM-3 attenuated cellular and prevented mitochondrial O<sub>2</sub><sup>-</sup> production. This indicates that mitochondria are the main source of HGHF-induced O<sub>2</sub><sup>-</sup> production.

Due to the link between mitochondrial oxidant production and inflammation (53), we measured the expression level of

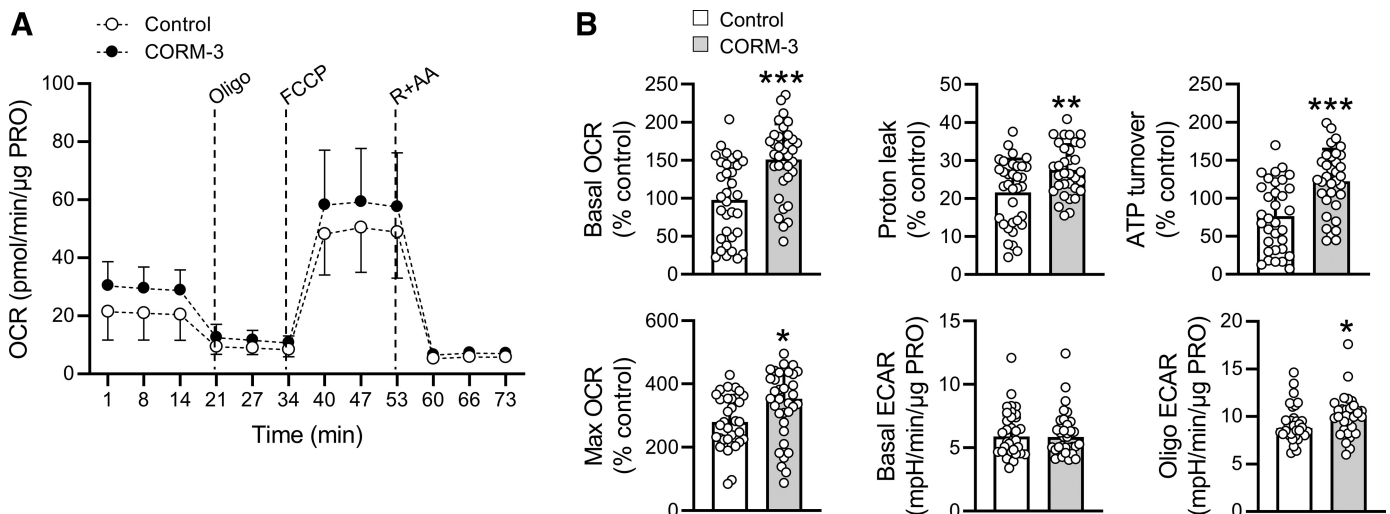


Fig. 4. Carbon monoxide-releasing molecule 3 (CORM-3) increases mitochondrial respiration and maximal glycolysis in C2C12 cells acutely exposed to high glucose and high fat (HGHF). *A*: cells were incubated in low glucose (LG) (5.6 mM) and treated with 20  $\mu$ M of CORM-3 or iCORM (control) for 4 h (*experiment 1*). Immediately before we performed a Mito Stress test with a Seahorse XFe96 Analyzer, 10 mM glucose (total 15.6 mM), 250  $\mu$ M of BSA-palmitate, 1 mM L-carnitine hydrochloride, and 100 nM insulin were added to the cells. Three measurements of oxygen consumption rates (OCRs) and extracellular acidification rates (ECARs) were made at baseline and after the addition of 2  $\mu$ M of oligomycin A (Oligo), 2  $\mu$ M FCCP, and 1  $\mu$ M rotenone and antimycin A (R + AA). *B*: data are presented as individual data points (%baseline control) from 3 independent experiments with means  $\pm$  SD bars (basal OCR, proton leak, and ATP turnover) or medians and interquartile range (Q1–Q3) (max OCR, basal ECAR, and oligomycin A ECAR) due to nonnormal data distribution ( $n = 33$ – $35$ /group). Data were analyzed using a *t* test or Mann-Whitney rank sum test. Significantly different from control: \* $P < 0.05$ , \*\* $P < 0.01$ , \*\*\* $P < 0.001$ .

IL-10 protein due to its role in protecting skeletal muscle from diet-induced inflammation, insulin resistance, and glucose intolerance (13, 24) and because CO enhances IL-10 production (33). Independent of treatment, HGHF led to increased IL-10 protein expression (Fig. 1C), suggesting an early counterinflammatory response to nutrient overload.

**CORM-3 and mitochondrial morphological alterations induced by HGHF in C2C12 cells.** HGHF increased mitochondrial fragmentation while reducing tubular and elongated network, and CORM-3 attenuated these morphological changes (Fig. 2A). OPA1 protein expression was not altered by condition or treatment, however, Mfn2 increased by 64% in CORM-3 treated cells (Fig. 2B). A trend for a lower Mfn2 was observed in HGHF cells ( $P = 0.057$ ). CORM-3 repressed the HGHF-induced expression of Drp1 by 76% (Fig. 2C). Due to the level of change in Drp1 and its regulatory role in fission, we further explored its location, i.e., cytosol or mitochondria (Fig. 2D). In LG cells, the majority of Drp1 is diffusely expressed in the cytosol. In contrast, HGHF increased Drp1 in puncta of fragmented mitochondria, whereas CORM-3 prevented Drp1 mediated fragmentation.

**CORM-3 and mitochondrial mass and mitophagy regulation in C2C12 cells.** In HGHF cells, mitochondrial mass was reduced by 27% (Fig. 3A). CORM-3 increased mitochondrial mass by 31% in LG cells and prevented the HGHF-induced reduction in mass. The protein expression of citrate synthase was similarly reduced by HGHF and increased by CORM-3 (Fig. 3B). The protein levels of regulators (PGC-1 $\alpha$  and TFAM) and indicators (subunits of mitochondrial complexes I-V) of mitochondrial biogenesis were unchanged during the 4-h experiments (Fig. 3C). While the mitophagy protein parkin was unaffected by condition or treatment, CORM-3 suppressed a 45% increase in HGHF-induced PINK1 protein expression (Fig. 3D). This suggests that the changes in mitochondrial mass are due to complementation rather than mitophagy and or mitochondrial biogenesis.

**CORM-3 and respiration,  $\Delta\Psi_m$ , and intramyocellular lipid content in C2C12 cells.** In experiment 1, cells were incubated in LG media with 20  $\mu$ M of CORM-3 or iCORM-3 (control) for 4 h and then exposed to HGHF during the respiratory control measurements (Fig. 4A). CORM-3 increased basal respiration, which is primarily controlled by ATP turnover,

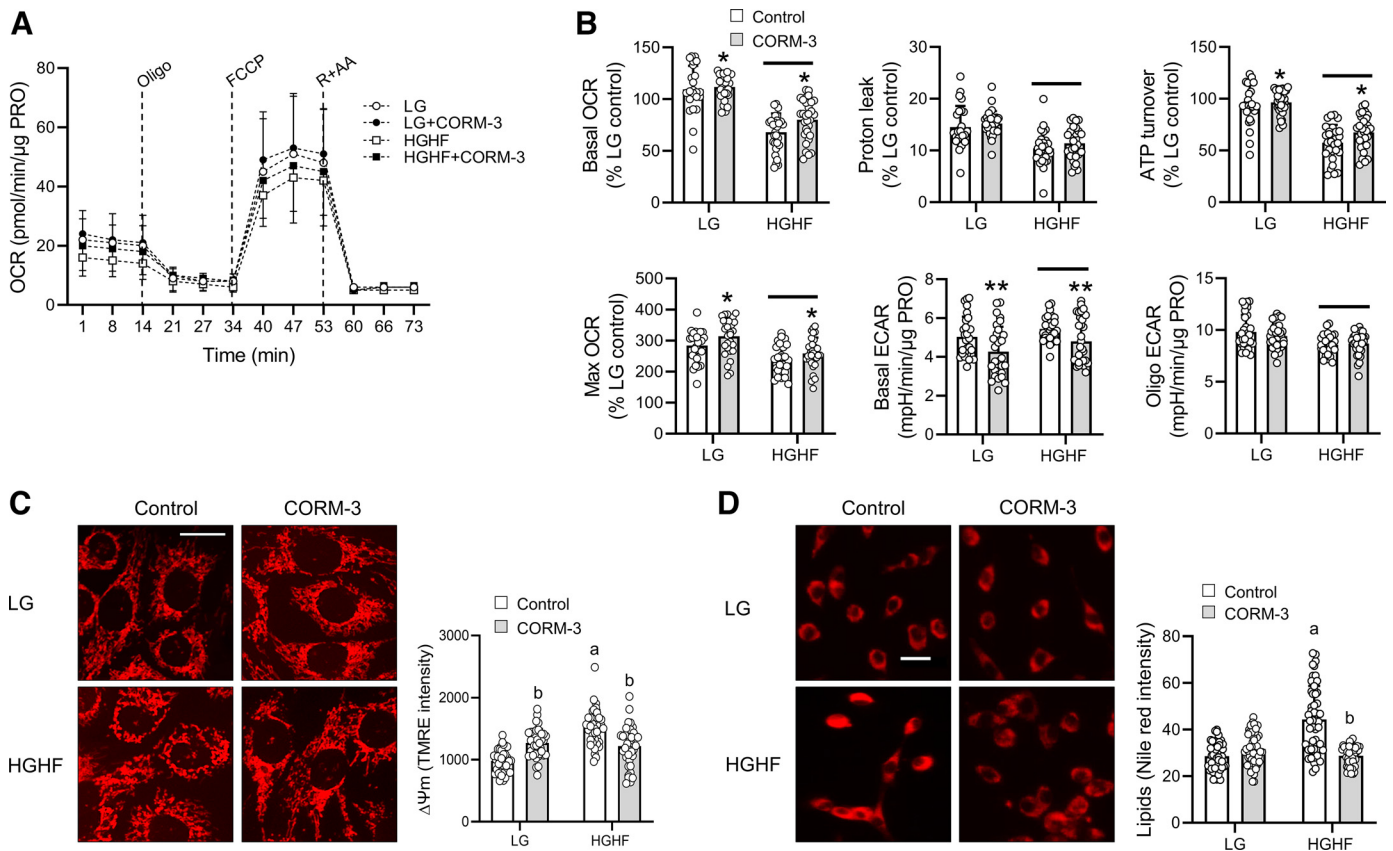


**Fig. 5.** Carbon monoxide-releasing molecule 3 (CORM-3) increases mitochondrial respiration and suppresses the high-glucose and high-fat (HGHF)-induced increase in  $\Delta\Psi_m$  and intramyocellular lipid accumulation in C2C12 cells. **A:** cells were incubated with either low glucose (LG) (5.6 mM) or HGHF (15.6 mM, 250  $\mu$ M) supplemented with 1 mM L-carnitine hydrochloride and 100 nM insulin, and treated with 20  $\mu$ M CORM or iCORM (control) for 4 h (experiment 2). Cells were exposed to Seahorse XF base medium supplemented with 5.6 mM glucose, 1 mM sodium pyruvate, and 4 mM glutamine during a Mito Stress test. Three measurements of oxygen consumption rates (OCRs) and extracellular acidification rates (ECARs) were made at baseline and after the addition of 2  $\mu$ M of oligomycin A, 2  $\mu$ M FCCP, and 1  $\mu$ M rotenone and antimycin A (R + AA). **B:** data are presented as individual data points (%baseline LG control) from 2 independent experiments with means  $\pm$  SD bars ( $n = 28$ –30/group). **C:** representative fluorescent images ( $\times 10$  magnification; scale bar = 10  $\mu$ m) of cells labeled with tetramethylrhodamine ethyl ester (TMRE).  $\Delta\Psi_m$  was measured by quantifying the fluorescence intensity of TMRE in 40 cells from 4 sections/group. **D:** representative fluorescent images ( $\times 10$  magnification; scale bar = 10  $\mu$ m) of cells labeled with Nile red. Intramyocellular lipid content was determined by quantifying the fluorescence intensity of Nile red in 50 cells from 5 sections/group. Data are presented as individual data points from 1 of 3 independent experiments with means  $\pm$  SD bars. Data were analyzed using a two-way ANOVA with Holm-Sidak test. Significant main effect of condition, treatment, and condition  $\times$  treatment: line = condition ( $P < 0.001$ ); \*treatment (\* $P < 0.05$ , \*\* $P < 0.01$ ); <sup>a</sup>condition within treatment and <sup>b</sup>treatment within condition ( $P < 0.001$ ).

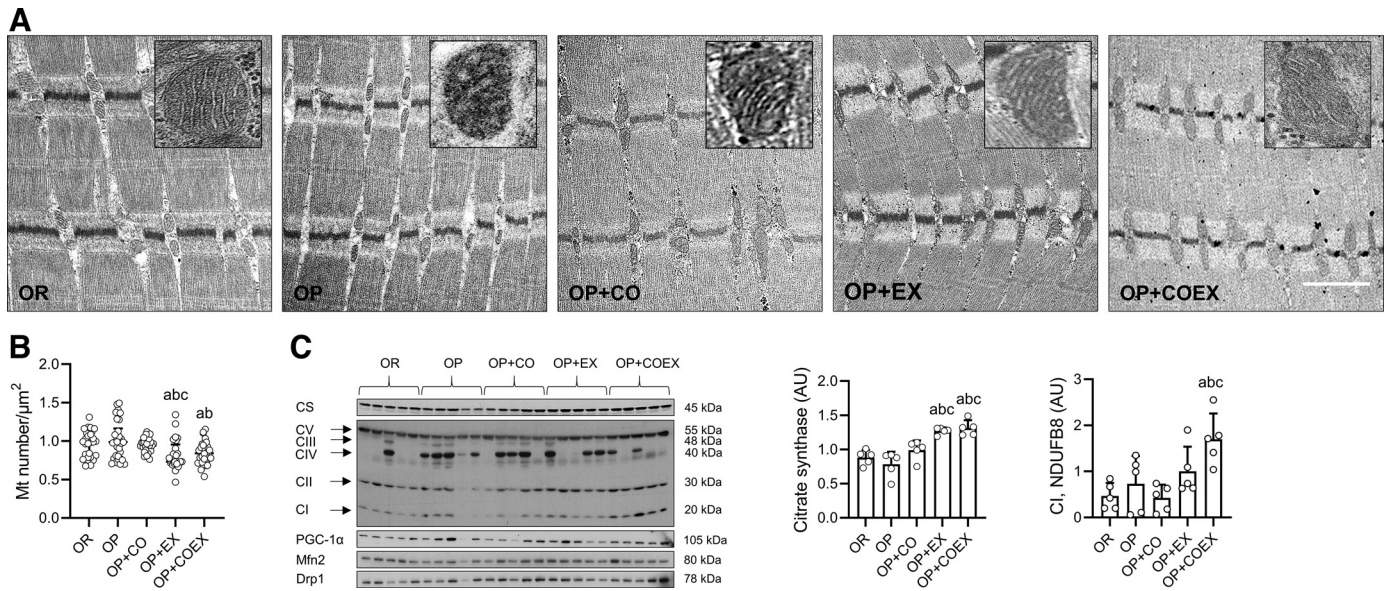


Fig. 6. Intermyo-fibrillar mitochondrial morphology, distribution, and regulation of biogenesis and dynamics in the rat soleus muscle fibers after a 10-wk diet-induced obesity study. *A*: representative soleus intermyofibrillar cross-sectional images obtained using transmission electron microscopy (magnification:  $\times 15,000$ ; insets:  $\times 50,000$ ). OR, obesity resistant; OP, obesity prone; CO, carbon monoxide; EX, exercise. *B*: mitochondrial number was determined by analyzing 10 different regions/animal ( $n = 30$ /group) at  $12,000$ – $15,000\times$  magnification using ImageJ. Data were analyzed using a Kruskal-Wallis one-way ANOVA with Tukey test and are presented as individual data points with medians and interquartile range (Q1–Q3). *C*: representative immunoblots of citrate synthase (CS), mitochondrial complexes I–V subunits, peroxisome proliferator-activated receptor  $\gamma$ -coactivator 1 $\alpha$  (PGC-1 $\alpha$ ), mitofusion 2 (Mfn2), and dynamin-related protein 1 (Drp1) [densitometry only shown for citrate synthase and complex I (CI) NDUFB8 subunit normalized to total protein]. AU, arbitrary units. Data from 5 to 8 rats/group were analyzed using a one-way ANOVA with Holm-Sidak test and are presented as means  $\pm$  SD. Significantly different from <sup>a</sup>OR, <sup>b</sup>OP, and <sup>c</sup>OP + CO rats,  $P < 0.001$  for electron microscopy and  $P < 0.05$  for citrate synthase and complex I NDUFB8.

proton leak, ATP turnover, and the maximal respiration rate induced by FCCP, which represents the maximum activity of electron transport and substrate oxidation (36) (Fig. 4B). CORM-3 also increased the maximal glycolytic rate by 13%. In *experiment 2*, cells were incubated in LG or HGHF media and treated with 20  $\mu$ M of CORM-3 or iCORM-3 for 4 h (Fig. 5A). HGHF reduced basal respiration, proton leak, ATP turnover, and maximal uncoupled respiration (Fig. 5B). CORM-3 increased basal respiration, ATP turnover, and FCCP-stimulated respiration. HGHF increased basal (10%) but not maximal glycolysis, and CORM-3 reduced the basal glycolytic rate by 16%. Thus CORM-3 improves ATP demand and substrate oxidation.

Using the same protocol in *experiment 2*, we measured  $\Delta\Psi_m$  and observed a 55% increase in HGHF cells (Fig. 5C). While CORM-3 increased  $\Delta\Psi_m$  by 30% in LG cells, the response in HGHF cells was suppressed. Since basal respiration was increased and basal glycolysis was reduced with CORM-3, we examined intramyocellular lipid content using

Nile red stain. HGHF increased intracellular lipid content by 55%, but CORM-3 prevented this accumulation. This provides further support for CORM-3 increasing substrate oxidation while reducing  $O_2^{\cdot-}$  production and suggests increased lipid oxidation.

*CO and moderate exercise training on skeletal muscle mitochondrial morphology, dynamic regulation, and biogenesis in rats during diet-induced obesity.* Transmission electron microscopic images of the soleus muscle are shown in Fig. 6A and mitochondrial morphological parameters in Table 1. In comparison with OR rats, diet-induced obesity led to reduced mitochondrial size, shape and complexity, and the cristae were without distinct organization (Fig. 6A, insets). Intermittent low-dose inhaled carbon monoxide offered no protection against these effects of diet-induced obesity on mitochondrial morphology. Despite a reduction in the distribution of mitochondria, exercise increased mitochondrial size and citrate synthase protein expression (Fig. 5C), thus density, and morphological parameters. Combining CO with exercise led to

Table 1. Rat soleus intermyofibrillar mitochondrial morphology

|                            | OR               | OP                            | OP + CO                         | OP + EX                           | OP + COEX                           |
|----------------------------|------------------|-------------------------------|---------------------------------|-----------------------------------|-------------------------------------|
| Length, $\mu$ m            | 0.38 (0.28–0.51) | 0.33 (0.26–0.41) <sup>a</sup> | 0.27 (0.23–0.34) <sup>a,b</sup> | 0.35 (0.29–0.44) <sup>a,b,c</sup> | 0.41 (0.33–0.52) <sup>a,b,c,d</sup> |
| Area, $\mu$ m <sup>2</sup> | 0.05 (0.04–0.07) | 0.04 (0.03–0.06) <sup>a</sup> | 0.03 (0.02–0.05) <sup>a,b</sup> | 0.06 (0.04–0.08) <sup>a,b,c</sup> | 0.07 (0.05–0.10) <sup>a,b,c,d</sup> |
| Perimeter, $\mu$ m         | 0.96 (0.77–1.22) | 0.82 (0.66–1.04) <sup>a</sup> | 0.72 (0.61–0.86) <sup>a,b</sup> | 0.94 (0.78–1.17) <sup>b,c</sup>   | 1.07 (0.90–1.29) <sup>a,b,c,d</sup> |
| Circularity, 0–1           | 0.73 (0.56–0.85) | 0.77 (0.67–0.84) <sup>a</sup> | 0.82 (0.75–0.88) <sup>a,b</sup> | 0.81 (0.72–0.88) <sup>a,b</sup>   | 0.79 (0.68–0.85) <sup>a,c,d</sup>   |
| Feret’s diameter           | 0.38 (0.28–0.50) | 0.33 (0.26–0.42) <sup>a</sup> | 0.27 (0.23–0.34) <sup>a,b</sup> | 0.36 (0.29–0.46) <sup>b,c</sup>   | 0.41 (0.34–0.52) <sup>a,b,c,d</sup> |
| Form factor                | 1.38 (1.18–1.77) | 1.31 (1.19–1.49) <sup>a</sup> | 1.22 (1.14–1.34) <sup>a,b</sup> | 1.23 (1.14–1.39) <sup>a,b</sup>   | 1.27 (1.18–1.46) <sup>a,c,d</sup>   |
| Aspect ratio               | 2.03 (1.54–2.96) | 1.99 (1.64–2.44)              | 1.70 (1.46–2.05) <sup>a,b</sup> | 1.70 (1.40–2.13) <sup>a,b</sup>   | 1.86 (1.53–2.32) <sup>a,b,c,d</sup> |

Values are medians and interquartile range (Q1–Q3) in parentheses. Significantly different from <sup>a</sup>obese resistant (OR), <sup>b</sup>obese prone (OP), <sup>c</sup>obese prone + carbon monoxide (OP + CO), and <sup>d</sup>obese prone + exercise (OP + EX) rats (Kruskal-Wallis one-way ANOVA with Tukey test),  $P < 0.001$ .

further improvements in mitochondrial morphology (compared with exercise, Cohen's  $d \geq 0.2$ – $0.3$ ) and increased complex I NDUFB8 protein expression. The responses were not accompanied by changes in the protein expression of PGC-1 $\alpha$ , Mfn2, Drp1 (Fig. 5C), or IL-10 (data not shown). This implies that the combination of CO and exercise helps preserve mitochondrial morphology during periods of nutrient excess.

*CO and moderate exercise training on skeletal muscle respiration and energy expenditure in rats during diet-induced obesity.* NADH-supported leak respiration did not differ among groups (Fig. 7A). When a saturating amount of ADP was added to these fibers, combined CO and exercise increased oxygen consumption by 158% over OR rats. Leak control ratio did not differ among groups nor did maximal fat oxidation. Diet-induced obesity did result in reduced  $\dot{V}O_2$  ( $-34\%$ ),  $\dot{V}CO_2$  ( $-37\%$ ), and resting energy expenditure ( $-34\%$ ), and only combined CO and exercise prevented a decline in resting metabolic rate (Fig. 7B). Moreover, these animals trended to run further ( $+75$  m) and for a longer ( $+3$  min) than did the exercise only rats (Fig. 7C). This supports a beneficial role of CO and exercise in influencing skeletal muscle and whole body bioenergetics.

## DISCUSSION

Mitochondrial morphology is controlled by fusion and fission. Nutrient excess promotes fission and causes uncon-

strained fragmentation and impairs oxidative phosphorylation (51). This led us to explore whether CO could prevent these mitochondrial effects of nutrient excess. Our findings indicate that CO maintains the tubular and elongated mitochondrial network and prevents fragmentation mediated by Drp1, reduces mitochondrial  $O_2^-$  production, and increases respiration in C2C12 mouse myoblasts exposed to high-glucose and high-fat for 4 h. Moreover, in rats consuming a high-fat and high-sucrose diet for 10 wk, intermittent low-dose inhaled CO combined with moderate aerobic exercise training improves skeletal muscle mitochondrial morphology, increases ADP-stimulated respiration in permeabilized muscle fibers in the presence of pyruvate, and increases energy expenditure. Collectively, these data demonstrate a positive effect of CO and exercise in modulating skeletal muscle bioenergetics that is associated with steady mitochondrial dynamics during periods of nutrient overload.

Under most basal conditions, oxidative metabolism in skeletal muscle is primarily fueled by lipids (1). A shift occurs with feeding, such that that glucose oxidation and lipid storage increases while  $\beta$ -oxidation decreases (21). In diet-induced obesity, skeletal muscle develops insulin resistance, and the fasted- to fed-state shift in substrate oxidation is impaired and  $\beta$ -oxidation predominates (30). Increased availability of reducing equivalents (NADH and  $FADH_2$ ) to skeletal muscle mitochondria in the absence of ATP demand results in a reduction

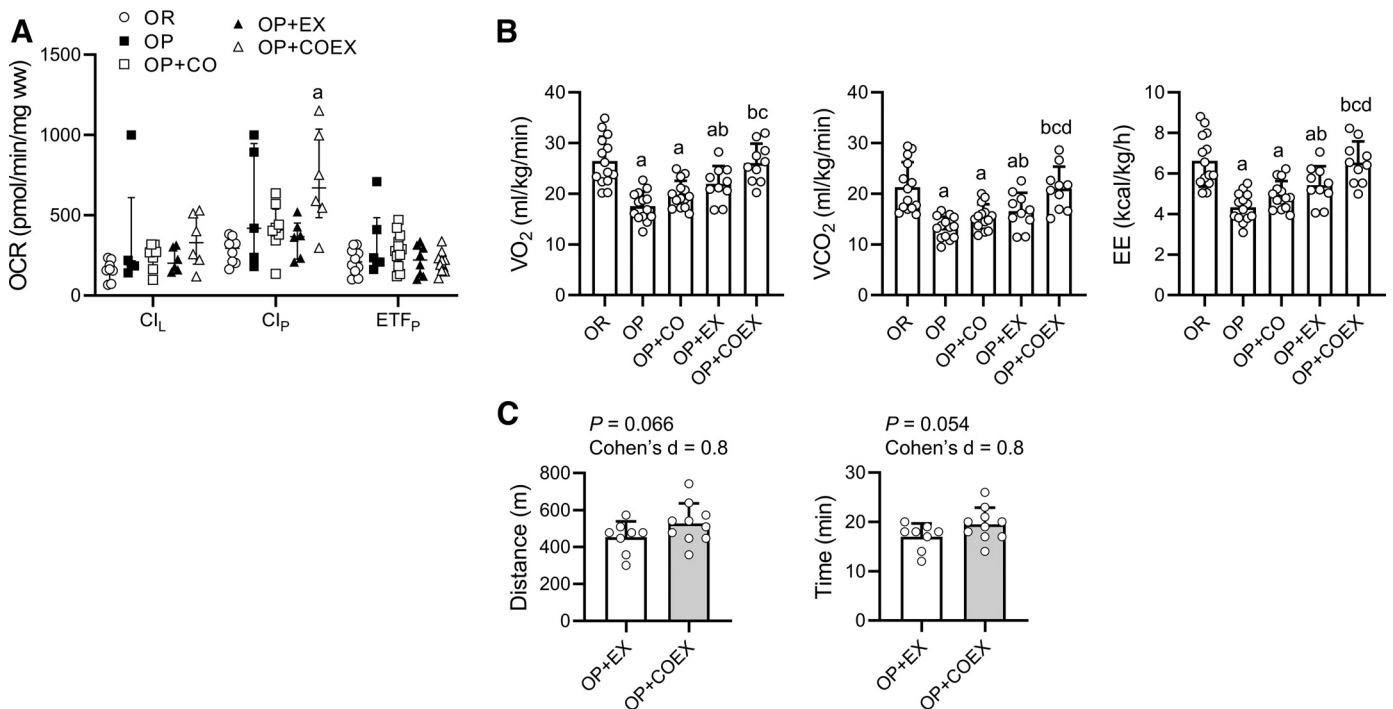


Fig. 7. Carbon monoxide (CO) and moderate aerobic exercise increase state 3 respiration in soleus muscle fibers and energy expenditure in rats after a 10-wk diet-induced obesity study. *A*: leak respiration in the presence of NADH-linked substrates (CI<sub>L</sub>, 5 mM malate, and 10 mM sodium pyruvate before the addition of 5 mM ADP (CI<sub>P</sub>, state 3). OR, obesity resistant; OP, obesity prone; CO, carbon monoxide; EX, exercise. Maximal fat oxidation induced by 50  $\mu$ M palmitoyl L-carnitine chloride + 5 mM ADP (ETF<sub>P</sub>). *B*: leak respiration in the presence of 5 mM malate and 50  $\mu$ M palmitoyl-L-carnitine chloride before the addition of 5 mM ADP (maximal fatty acid oxidative capacity). Data from 5 to 12 rats/group were analyzed using a Kruskal-Wallis one-way ANOVA with Dunn's test and are presented as individual data points with medians and interquartile range (Q1–Q3). Significantly different from <sup>a</sup>OR rats,  $P < 0.01$ . *C*: open circuit spirometry was determined over  $\sim 20$  min at the beginning of their dark cycles.  $\dot{V}O_2$ ,  $\dot{V}CO_2$ , and energy expenditure (product of calorific value and  $\dot{V}O_2$ ). Data from 10 to 15 rats/group were analyzed using a one-way ANOVA with Holm-Sidak test, and presented as individual data points with means  $\pm$  SD. Significantly different from <sup>a</sup>OR, <sup>b</sup>OP, <sup>c</sup>OP + CO, and <sup>d</sup>OP + EX rats,  $P < 0.001$ . *D*: a run to exhaustion test in OP + EX and OP + COEX rats after the 10-wk diet-induced obesity study. Data are presented as individual data points ( $n = 8$ – $10$  animals/group) with means  $\pm$  SD bars.

in respiratory capacity that is accompanied by increased oxidant production, an initial increase in  $\Delta\Psi_m$  that eventually falls, and mitochondrial fission and fragmentation that are modulated by the GTPase fission and fusion proteins Drp1 and Mfn2. Fragmented mitochondria may fuse if membrane potential recovers (31), but if mitochondria remain depolarized, PINK1 accumulates in mitochondria and phosphorylates the E3 ubiquitin ligase parkin, resulting in outer mitochondrial membrane ubiquitination and mitophagy (39).

Here, HGHF increased mitochondrial  $O_2^-$  production,  $\Delta\Psi_m$ , mitochondrial fission, and fragmentation that was mediated by increased Drp1 expression and recruitment to mitochondria and reduced mitochondrial mass; these alterations were accompanied by a reduction in respiration and increased intramyocellular lipid accumulation. The increase in PINK1 and a trend for lower Mfn2 without an increase parkin suggests full activation of mitophagy had not occurred, i.e., PINK1 phosphorylates Mfn2, which becomes ubiquitinated by parkin (10). This may occur if the mitochondria were still hyperpolarized and inflammation was not involved, suggesting an early phase of metabolic overload. Alternatively, mitophagy could have been initiated by PINK1/parkin-independent mechanisms (18, 39), yet a response in mitochondrial biogenesis would have been expected as reported for longer exposure protocols (28, 38, 40).

CO has been reported to reduce weight gain and adiposity, glucose intolerance and insulin resistance, and hyperleptinemia in mice consuming high-fat diets (6, 26, 27, 57). The mechanism for the anti-obesity effects remains unknown; however, uncoupled respiration in adipocytes has been proposed (27). Under resting conditions *in vivo*, ADP phosphorylation accounts for ~90% of oxygen consumption in skeletal muscle (35), and 86% in our *in vitro* experiment, representing highly coupled respiration. Thus, excess proton conductance in skeletal muscle mitochondrion may not be useful, specifically during periods of high-energy demands such as muscular contraction. Moreover, CO binds only to cytochrome  $a_3$  of cytochrome *c* oxidase (47), raising the question of how this leads to uncoupled respiration. In our study, when cells were exposed to LG during the respiration measurements (*experiment 2*), CORM-3 increased basal respiration and ATP turnover without altering proton leak, and  $\Delta\Psi_m$  was maintained. This observation may be related to morphological changes mediated by Mfn2 and Drp1 because tubular and elongated mitochondria possess a greater respiratory capacity than fragmented mitochondria in skeletal muscle cells (38). The increased ATP demand associated with mitochondrial elongation would require an increase in coupled respiration. In cells treated with CORM-3 before exposure to HGHF during the respiration measurements, representing a postprandial state (*experiment 1*), proton leak was elevated, indicating more uncoupled respiration. Since we did not measure  $\Delta\Psi_m$  in these cells, the degree of uncoupling cannot be established. It is worth noting that coupling efficiency was perhaps marginally improved in CORM-3 treated cells (4.2%,  $P = 0.055$ ) due to a higher ATP turnover rate. The possibility of CORM-3 increasing uncoupled respiration (32, 37) was not supported in our experiments with immortalized mouse myoblasts, which favored an increase in coupled respiration to meet ATP demand, similarly reported in HepG2 cells incubated in palmitate

and treated with CORM-A1 (50). Measurement of the local P/O ratio may have supported this assertion.

In obesity and diabetes, skeletal muscle mitochondria are smaller and shorter, unevenly distributed with a disorganized pattern, and show sparse cristae (4, 15, 28, 29). We observed a similar mitochondrial morphological profile in the soleus of OP rats that consumed a high-fat and high-sucrose diet for 10 wk. Despite these changes and a reduction in whole body energy expenditure, permeabilized muscle fiber respiration supported by pyruvate or palmitate was unaffected by diet-induced obesity. This is likely because mitochondrial distribution and citrate synthase expression were maintained, indicating an adequate number of functioning mitochondria. Similar to our cell experiments, the duration of the diet intervention was relatively short and did not lead to systemic and tissue inflammation, supported by unchanged plasma C-reactive protein (19) and muscle IL-10 protein expression. These data, therefore, represent an early phase of diet-induced obesity when skeletal muscle mitochondria are first adapting to nutrient stress.

Instead of delivering CO via carbon monoxide-releasing molecules (CO-RMs), rats were pretreated with low-dose inhaled CO at 250 ppm for 1 h for 5 days, and biweekly for 10 wk because low-dose CO inhalation has been safety-tested in a phase I clinical trial (17). The CO-dosing strategy used here was ineffective for preserving mitochondrial morphology during chronic overfeeding. The combination of CO and exercise, however, led to robust changes in mitochondrial morphology. In addition, ADP-stimulated respiration in the presence of pyruvate was increased over OR lean rats, and this was accompanied by an increased expression of the complex I anchoring protein (NDUFB8). Moreover, the reduced energy expenditure resulting from high-fat and high-sucrose feeding was prevented in OP + COEX rats. It is probable that other tissues contributed to this increase in metabolic rate, e.g., liver and brown adipose tissue. While measuring aerobic exercise performance was not an objective of this study, rats that received CO and underwent exercise training trended to run further and for a longer time. This highlights the potential benefits of combining two treatments that may allow for lower doses of both to be prescribed; however, the precise mechanisms for these responses remain to be determined. Measurement of tissue CO levels, which vary considerably (43), would assist in developing effective treatment regimens while avoiding toxicity.

Our findings identify a new role for CO in modulating skeletal muscle mitochondrial morphology and bioenergetics in conditions when nutrient supply exceeds cellular energy demand. CO delivered by CORM-3 reduced mitochondrial fragmentation and  $O_2^-$  production induced by nutrient excess, and this was accompanied by an increase in respiratory capacity rather than an increase in uncoupling. When CO was inhaled and combined with moderate aerobic exercise, the consequences of chronic nutrient stress on skeletal muscle mitochondrial morphology and resting energy expenditure were prevented. The mechanism(s) for the observed responses to CO, and whether respiratory stress leads to morphological changes, or vice versa, were not ascertained here, but these data identify a new direction in the capacity of CO to prevent the complications of nutrient excess.

## ACKNOWLEDGMENTS

We thank Dr. Dennis McDaniel, Pauline Peacock, and Jenna Hagin (Uniformed Services University of the Health Sciences), May Guo (Seahorse Instruments), and Martha Salinas (Duke University) for technical assistance.

## GRANTS

This research was supported by the Uniformed Services University of the Health Sciences Office of Research.

## DISCLAIMERS

The views expressed are those of the authors and do not reflect the official position of the Uniformed Services University of the Health Sciences, United States Navy, or United States Department of Defense.

## DISCLOSURES

No conflicts of interest, financial or otherwise, are declared by the authors.

## AUTHOR CONTRIBUTIONS

H.G.G. and T.Y. conceived and designed research; H.G.G., J.D., and T.Y. performed experiments; H.G.G., J.D., H.B.S., and T.Y. analyzed data; H.G.G., H.B.S., C.A.P., and T.Y. interpreted results of experiments; H.G.G., H.B.S., and T.Y. prepared figures; H.G.G. drafted manuscript; H.G.G., H.B.S., C.A.P., and T.Y. edited and revised manuscript; H.G.G., J.D., H.B.S., C.A.P., and T.Y. approved final version of manuscript.

## REFERENCES

- Andres R, Cader G, Zierler KL. The quantitatively minor role of carbohydrate in oxidative metabolism by skeletal muscle in intact man in the basal state; measurements of oxygen and glucose uptake and carbon dioxide and lactate production in the forearm. *J Clin Invest* 35: 671–682, 1956. doi:10.1172/JCI103324.
- Archer SL. Mitochondrial dynamics—mitochondrial fission and fusion in human diseases. *N Engl J Med* 369: 2236–2251, 2013. doi:10.1056/NEJMr1215233.
- Bach D, Pich S, Soriano FX, Vega N, Baumgartner B, Oriola J, Daugaard JR, Lloberas J, Camps M, Zierath JR, Rabasa-Lhoret R, Wallberg-Henriksson H, Laville M, Palacín M, Vidal H, Rivera F, Brand M, Zorzano A. Mitofusin-2 determines mitochondrial network architecture and mitochondrial metabolism. A novel regulatory mechanism altered in obesity. *J Biol Chem* 278: 17190–17197, 2003. doi:10.1074/jbc.M212754200.
- Bonnard C, Durand A, Peyrol S, Chanseaux E, Chauvin MA, Morio B, Vidal H, Rieusset J. Mitochondrial dysfunction results from oxidative stress in the skeletal muscle of diet-induced insulin-resistant mice. *J Clin Invest* 118: 789–800, 2008. doi:10.1172/JCI32601.
- Brand MD, Nicholls DG. Assessing mitochondrial dysfunction in cells. *Biochem J* 435: 297–312, 2011. doi:10.1042/BJ20110162.
- Braud L, Pini M, Muchova L, Manin S, Kitagishi H, Sawaki D, Czibik G, Ternacle J, Derumeaux G, Foresti R, Motterlini R. Carbon monoxide-induced metabolic switch in adipocytes improves insulin resistance in obese mice. *JCI Insight* 3: e123485, 2018. doi:10.1172/jci.insight.123485.
- Brown SD, Piantadosi CA. In vivo binding of carbon monoxide to cytochrome c oxidase in rat brain. *J Appl Physiol* (1985) 68: 604–610, 1990. doi:10.1152/jappl.1990.68.2.604.
- Brown SD, Piantadosi CA. Recovery of energy metabolism in rat brain after carbon monoxide hypoxia. *J Clin Invest* 89: 666–672, 1992. doi:10.1172/JCI115633.
- Cefalu WT, Bray GA, Home PD, Garvey WT, Klein S, Pi-Sunyer FX, Hu FB, Raz I, Van Gaal L, Wolfe BM, Ryan DH. Advances in the science, treatment, and prevention of the disease of obesity: reflections from a *Diabetes Care* Editors' Expert Forum. *Diabetes Care* 38: 1567–1582, 2015. doi:10.2337/dc15-1081.
- Chen Y, Dorn GW 2nd. PINK1-phosphorylated mitofusin 2 is a Parkin receptor for culling damaged mitochondria. *Science* 340: 471–475, 2013. doi:10.1126/science.1231031.
- Clark JE, Naughton P, Shurey S, Green CJ, Johnson TR, Mann BE, Foresti R, Motterlini R. Cardioprotective actions by a water-soluble carbon monoxide-releasing molecule. *Circ Res* 93: e2–e8, 2003. doi:10.1161/01.RES.0000084381.86567.08.
- Coburn RF. Mechanisms of carbon monoxide toxicity. *Prev Med* 8: 310–322, 1979. doi:10.1016/0091-7435(79)90008-2.
- Dagdeviren S, Jung DY, Lee E, Friedline RH, Noh HL, Kim JH, Patel PR, Tsitsilianos N, Tsitsilianos AV, Tran DA, Tsougranis GH, Kearns CC, Uong CP, Kwon JY, Muller W, Lee KW, Kim JK. Altered interleukin-10 signaling in skeletal muscle regulates obesity-mediated inflammation and insulin resistance. *Mol Cell Biol* 36: 2956–2966, 2016. doi:10.1128/MCB.00181-16.
- Dell'Anna ML, Ottaviani M, Kovacs D, Mirabilli S, Brown DA, Cota C, Migliano E, Bastonini E, Bellei B, Cardinali G, Ricciardi MR, Tafuri A, Picardo M. Energetic mitochondrial failing in vitiligo and possible rescue by cardiopilin. *Sci Rep* 7: 13663, 2017. doi:10.1038/s41598-017-13961-5.
- Dohl J, Foldi J, Heller J, Gasier HG, Deuster PA, Yu T. Acclimation of C<sub>2</sub>C<sub>12</sub> myoblasts to physiological glucose concentrations for in vitro diabetes research. *Life Sci* 211: 238–244, 2018. doi:10.1016/j.lfs.2018.09.041.
- Fredenburgh LE, Kraft BD, Hess DR, Harris RS, Wolf MA, Suliman HB, Roggli VL, Davies JD, Winkler T, Stenzler A, Baron RM, Thompson BT, Choi AM, Welty-Wolf KE, Piantadosi CA. Effects of inhaled CO administration on acute lung injury in baboons with pneumococcal pneumonia. *Am J Physiol Lung Cell Mol Physiol* 309: L834–L846, 2015. doi:10.1152/ajplung.00240.2015.
- Fredenburgh LE, Perrella MA, Barragan-Bradford D, Hess DR, Peters E, Welty-Wolf KE, Kraft BD, Harris RS, Maurer R, Nakahira K, Oromendia C, Davies JD, Higuera A, Schiffer KT, Englert JA, Dieffenbach PB, Berlin DA, Lagambina S, Bouthot M, Sullivan AI, Nuccio PF, Kone MT, Malik MJ, Porras MA, Finkelsztein E, Winkler T, Hurwitz S, Serhan CN, Piantadosi CA, Baron RM, Thompson BT, Choi AM. A phase I trial of low-dose inhaled carbon monoxide in sepsis-induced ARDS. *JCI Insight* 3: e124039, 2018. doi:10.1172/jci.insight.124039.
- Fu T, Xu Z, Liu L, Guo Q, Wu H, Liang X, Zhou D, Xiao L, Liu L, Liu Y, Zhu MS, Chen Q, Gan Z. Mitophagy directs muscle-adipose crosstalk to alleviate dietary obesity. *Cell Reports* 23: 1357–1372, 2018. doi:10.1016/j.celrep.2018.03.127.
- Gasier HG, Yu T, Swift JM, Metzger CE, McNerny EM, Swallow EA, Piantadosi CA, Allen MR. Carbon monoxide and exercise prevents diet-induced obesity and metabolic dysregulation without affecting bone. *Obesity (Silver Spring)* 28: 924–931, 2020. doi:10.1002/oby.22768.
- Gomes LC, Di Benedetto G, Scorrano L. During autophagy mitochondria elongate, are spared from degradation and sustain cell viability. *Nat Cell Biol* 13: 589–598, 2011. doi:10.1038/ncb2220.
- Goodpaster BH, Sparks LM. Metabolic flexibility in health and disease. *Cell Metab* 25: 1027–1036, 2017. doi:10.1016/j.cmet.2017.04.015.
- Gustavsson N, Abedi G, Larsson-Nyrén G, Lindström P. Timing of Ca<sup>2+</sup> response in pancreatic β-cells is related to mitochondrial mass. *Biochem Biophys Res Commun* 340: 1119–1124, 2006. doi:10.1016/j.bbrc.2005.12.119.
- Harper JA, Dickinson K, Brand MD. Mitochondrial uncoupling as a target for drug development for the treatment of obesity. *Obes Rev* 2: 255–265, 2001. doi:10.1046/j.1467-789X.2001.00043.x.
- Hong EG, Ko HJ, Cho YR, Kim HJ, Ma Z, Yu TY, Friedline RH, Kurt-Jones E, Finberg R, Fischer MA, Granger EL, Norbury CC, Hauschka SD, Philbrick WM, Lee CG, Elias JA, Kim JK. Interleukin-10 prevents diet-induced insulin resistance by attenuating macrophage and cytokine response in skeletal muscle. *Diabetes* 58: 2525–2535, 2009. doi:10.2337/db08-1261.
- Hoppins S, Lackner L, Nunnari J. The machines that divide and fuse mitochondria. *Annu Rev Biochem* 76: 751–780, 2007. doi:10.1146/annurev.biochem.76.071905.090048.
- Hosick PA, AlAmodi AA, Hankins MW, Stec DE. Chronic treatment with a carbon monoxide releasing molecule reverses dietary induced obesity in mice. *Adipocyte* 5: 1–10, 2015. doi:10.1080/21623945.2015.1038443.
- Hosick PA, AlAmodi AA, Storm MV, Gousset MU, Pruett BE, Gray W 3rd, Stout J, Stec DE. Chronic carbon monoxide treatment attenuates development of obesity and remodels adipocytes in mice fed a high-fat diet. *Int J Obes* 38: 132–139, 2014. doi:10.1038/ijo.2013.61.
- Jheng HF, Tsai PJ, Guo SM, Kuo LH, Chang CS, Su IJ, Chang CR, Tsai YS. Mitochondrial fission contributes to mitochondrial dysfunction and insulin resistance in skeletal muscle. *Mol Cell Biol* 32: 309–319, 2012. doi:10.1128/MCB.05603-11.

29. Kelley DE, He J, Menshikova EV, Ritov VB. Dysfunction of mitochondria in human skeletal muscle in type 2 diabetes. *Diabetes* 51: 2944–2950, 2002. doi:10.2337/diabetes.51.10.2944.
30. Koves TR, Ussher JR, Noland RC, Slentz D, Mosedale M, Ilkayeva O, Bain J, Stevens R, Dyck JR, Newgard CB, Lopaschuk GD, Muoio DM. Mitochondrial overload and incomplete fatty acid oxidation contribute to skeletal muscle insulin resistance. *Cell Metab* 7: 45–56, 2008. doi:10.1016/j.cmet.2007.10.013.
31. Liesa M, Shirihai OS. Mitochondrial dynamics in the regulation of nutrient utilization and energy expenditure. *Cell Metab* 17: 491–506, 2013. doi:10.1016/j.cmet.2013.03.002.
32. Lo Iacono L, Boczkowski J, Zini R, Salouage I, Berdeaux A, Motterlini R, Morin D. A carbon monoxide-releasing molecule (CORM-3) uncouples mitochondrial respiration and modulates the production of reactive oxygen species. *Free Radic Biol Med* 50: 1556–1564, 2011. doi:10.1016/j.freeradbiomed.2011.02.033.
33. MacGarvey NC, Suliman HB, Bartz RR, Fu P, Withers CM, Welty-Wolf KE, Piantadosi CA. Activation of mitochondrial biogenesis by heme oxygenase-1-mediated NF-E2-related factor-2 induction rescues mice from lethal *Staphylococcus aureus* sepsis. *Am J Respir Crit Care Med* 185: 851–861, 2012. doi:10.1164/rccm.201106-1152OC.
34. Malka F, Guillery O, Cifuentes-Diaz C, Guillou E, Belenguer P, Lombès A, Rojo M. Separate fusion of outer and inner mitochondrial membranes. *EMBO Rep* 6: 853–859, 2005. doi:10.1038/sj.embor.7400488.
35. Marcinek DJ, Schenkman KA, Ciesielski WA, Conley KE. Mitochondrial coupling in vivo in mouse skeletal muscle. *Am J Physiol Cell Physiol* 286: C457–C463, 2004. doi:10.1152/ajpcell.00237.2003.
36. Mitra K, Wunder C, Roysam B, Lin G, Lippincott-Schwartz J. A hyperfused mitochondrial state achieved at G<sub>1</sub>-S regulates cyclin E buildup and entry into S phase. *Proc Natl Acad Sci USA* 106: 11960–11965, 2009. doi:10.1073/pnas.0904875106.
37. Motterlini R, Foresti R. Biological signaling by carbon monoxide and carbon monoxide-releasing molecules. *Am J Physiol Cell Physiol* 312: C302–C313, 2017. doi:10.1152/ajpcell.00360.2016.
38. Nisr RB, Shah DS, Ganley IG, Hundal HS. Proinflammatory NFκB signalling promotes mitochondrial dysfunction in skeletal muscle in response to cellular fuel overloading. *Cell Mol Life Sci* 76: 4887–4904, 2019. doi:10.1007/s00018-019-03148-8.
39. Palikaras K, Lionaki E, Tavernarakis N. Mechanisms of mitophagy in cellular homeostasis, physiology and pathology. *Nat Cell Biol* 20: 1013–1022, 2018. doi:10.1038/s41556-018-0176-2.
40. Patková J, Anděl M, Trnka J. Palmitate-induced cell death and mitochondrial respiratory dysfunction in myoblasts are not prevented by mitochondria-targeted antioxidants. *Cell Physiol Biochem* 33: 1439–1451, 2014. doi:10.1159/000358709.
41. Pecorella SR, Potter JV, Cherry AD, Peacher DF, Welty-Wolf KE, Moon RE, Piantadosi CA, Suliman HB. The HO-1/CO system regulates mitochondrial-capillary density relationships in human skeletal muscle. *Am J Physiol Lung Cell Mol Physiol* 309: L857–L871, 2015. doi:10.1152/ajplung.00104.2015.
42. Perry CG, Kane DA, Lin CT, Kozy R, Cathey BL, Lark DS, Kane CL, Brophy PM, Gavin TP, Anderson EJ, Neuffer PD. Inhibiting myosin-ATPase reveals a dynamic range of mitochondrial respiratory control in skeletal muscle. *Biochem J* 437: 215–222, 2011. doi:10.1042/BJ20110366.
43. Piantadosi CA. Carbon monoxide, reactive oxygen signaling, and oxidative stress. *Free Radic Biol Med* 45: 562–569, 2008. doi:10.1016/j.freeradbiomed.2008.05.013.
44. Piantadosi CA, Withers CM, Bartz RR, MacGarvey NC, Fu P, Sweeney TE, Welty-Wolf KE, Suliman HB. Heme oxygenase-1 couples activation of mitochondrial biogenesis to anti-inflammatory cytokine expression. *J Biol Chem* 286: 16374–16385, 2011. doi:10.1074/jbc.M110.207738.
45. Picard M, White K, Turnbull DM. Mitochondrial morphology, topology, and membrane interactions in skeletal muscle: a quantitative three-dimensional electron microscopy study. *J Appl Physiol (1985)* 114: 161–171, 2013. doi:10.1152/jappphysiol.01096.2012.
46. Smirnova E, Shurland DL, Ryazantsev SN, van der Blik AM. A human dynamin-related protein controls the distribution of mitochondria. *J Cell Biol* 143: 351–358, 1998. doi:10.1083/jcb.143.2.351.
47. Suliman HB, Carraway MS, Tatro LG, Piantadosi CA. A new activating role for CO in cardiac mitochondrial biogenesis. *J Cell Sci* 120: 299–308, 2007. doi:10.1242/jcs.03318.
48. Tao H, Zhang Y, Zeng X, Shulman GI, Jin S. Niclosamide ethanolate-induced mild mitochondrial uncoupling improves diabetic symptoms in mice. *Nat Med* 20: 1263–1269, 2014. doi:10.1038/nm.3699.
49. Tenhunen R, Marver HS, Schmid R. Microsomal heme oxygenase. Characterization of the enzyme. *J Biol Chem* 244: 6388–6394, 1969.
50. Upadhyay KK, Jadeja RN, Vyas HS, Pandya B, Joshi A, Vohra A, Thounaojam MC, Martin PM, Bartoli M, Devkar RV. Carbon monoxide releasing molecule-A1 improves nonalcoholic steatohepatitis via Nrf2 activation mediated improvement in oxidative stress and mitochondrial function. *Redox Biol* 28: 101314, 2020. doi:10.1016/j.redox.2019.101314.
51. Wai T, Langer T. Mitochondrial dynamics and metabolic regulation. *Trends Endocrinol Metab* 27: 105–117, 2016. doi:10.1016/j.tem.2015.12.001.
52. Wang YC, McPherson K, Marsh T, Gortmaker SL, Brown M. Health and economic burden of the projected obesity trends in the USA and the UK. *Lancet* 378: 815–825, 2011. doi:10.1016/S0140-6736(11)60814-3.
53. Yang S, Xia C, Li S, Du L, Zhang L, Zhou R. Defective mitophagy driven by dysregulation of rheb and KIF5B contributes to mitochondrial reactive oxygen species (ROS)-induced nod-like receptor 3 (NLRP3) dependent proinflammatory response and aggravates lipotoxicity. *Redox Biol* 3: 63–71, 2014. doi:10.1016/j.redox.2014.04.001.
54. Yoon Y, Krueger EW, Oswald BJ, McNiven MA. The mitochondrial protein hFis1 regulates mitochondrial fission in mammalian cells through an interaction with the dynamin-like protein DLP1. *Mol Cell Biol* 23: 5409–5420, 2003. doi:10.1128/MCB.23.15.5409-5420.2003.
55. Yu T, Robotham JL, Yoon Y. Increased production of reactive oxygen species in hyperglycemic conditions requires dynamic change of mitochondrial morphology. *Proc Natl Acad Sci USA* 103: 2653–2658, 2006. doi:10.1073/pnas.0511154103.
56. Zhang J, Piantadosi CA. Mitochondrial oxidative stress after carbon monoxide hypoxia in the rat brain. *J Clin Invest* 90: 1193–1199, 1992. doi:10.1172/JCI115980.
57. Zheng M, Zhang Q, Joe Y, Kim SK, Uddin MJ, Rhew H, Kim T, Ryter SW, Chung HT. Carbon monoxide-releasing molecules reverse leptin resistance induced by endoplasmic reticulum stress. *Am J Physiol Endocrinol Metab* 304: E780–E788, 2013. doi:10.1152/ajpendo.00466.2012.
58. Zorzano A, Liesa M, Palacín M. Role of mitochondrial dynamics proteins in the pathophysiology of obesity and type 2 diabetes. *Int J Biochem Cell Biol* 41: 1846–1854, 2009. doi:10.1016/j.biocel.2009.02.004.
59. Zuckerbraun BS, Chin BY, Bilban M, d'Avila JC, Rao J, Billiar TR, Otterbein LE. Carbon monoxide signals via inhibition of cytochrome c oxidase and generation of mitochondrial reactive oxygen species. *FASEB J* 21: 1099–1106, 2007. doi:10.1096/fj.06-6644com.

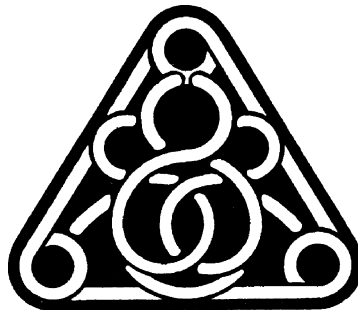
## CORRIGENDUM

**Gasier HG, Dohl J, Suliman HB, Piantadosi CA, Yu T.** Skeletal muscle mitochondrial fragmentation and impaired bioenergetics from nutrient overload are prevented by carbon monoxide. *Am J Physiol Cell Physiol* 319: C746–C756, 2020. First published August 26, 2020; <https://doi.org/10.1152/ajpcell.00016.2020>.—In the published version of this article, the RESULTS section “*CO and moderate exercise training on skeletal muscle mitochondrial morphology, dynamic regulation, and biogenesis in rats during diet-induced obesity*” refers to Fig. 5C when it should be Fig. 6, B and C. The two corrected sentences are as follows:

“Despite a reduction in the distribution of mitochondria, exercise increased mitochondrial size and citrate synthase protein expression (Fig. 6, B and C), thus density, and morphological parameters.”

“The responses were not accompanied by changes in the protein expression of PGC-1 $\alpha$ , Mfn2, Drp1 (Fig. 6, B and C), or IL-10 (data not shown).”

The revisions do not change the scientific conclusions of the study.



**CORRIGENDUM**

**Corrigendum for Gasier HG et al., volume 319, 2020, p. C746–C756**

**Gasier HG, Dohl J, Suliman HB, Piantadosi CA, Yu T.** Skeletal muscle mitochondrial fragmentation and impaired bioenergetics from nutrient overload are prevented by carbon monoxide. *Am J Physiol Cell Physiol* 319: C746–C756, 2020. First published August 26, 2020; doi:10.1152/ajpcell.00016.2020.

In the above article, Fig. 7 legend was published incorrectly. The corrected figure is shown below. The authors assert that the corrections do not affect the conclusions of the study.

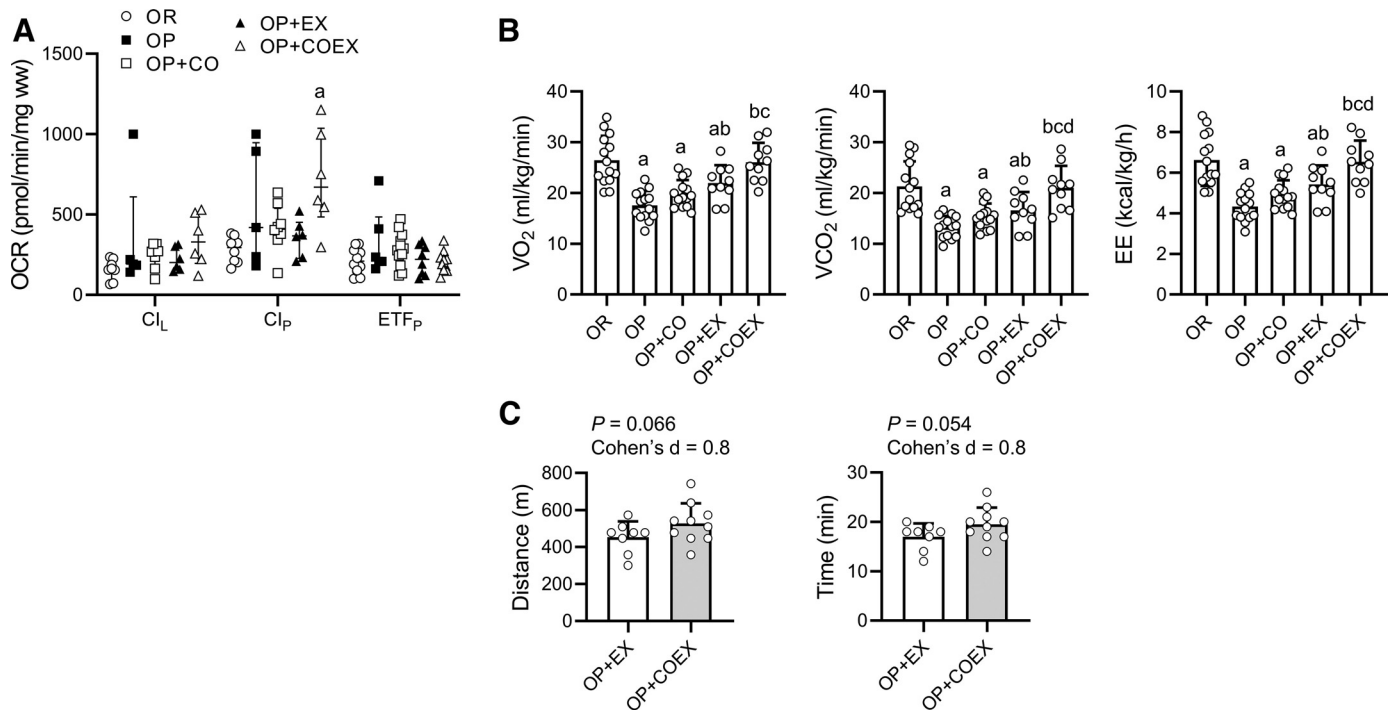


**Fig. 7.** Carbon monoxide (CO) and moderate aerobic exercise increase state 3 respiration in soleus muscle fibers and energy expenditure in rats after a 10-wk diet-induced obesity study. **A:** leak respiration in the presence of NADH-linked substrates (Cl<sub>L</sub>), 5 mM malate + 10 mM sodium pyruvate, prior to the addition of 5 mM ADP (Cl<sub>P</sub>, state 3). Maximal fat oxidation induced by 50 μM palmitoyl L-carnitine chloride + 5 mM ADP (ETF<sub>P</sub>). Data from 5–12 rats/group were analyzed using a Kruskal–Wallis one-way ANOVA with Dunn’s test, and presented as individual data points with medians and interquartile range (Q1–Q3). Significantly different from <sup>a</sup>OR rats,  $P < 0.01$ . **B:** open circuit spirometry was determined over ~20 min at the beginning of their dark cycles.  $\dot{V}O_2$ ,  $\dot{V}CO_2$ , and energy expenditure (product of calorific value and  $\dot{V}O_2$ ). Data from 10–15 rats/group were analyzed using a one-way ANOVA with Holm–Sidak test, and presented as individual data points with means  $\pm$  SD. Significantly different from <sup>a</sup>OR, <sup>b</sup>OP, <sup>c</sup>OP + CO, and <sup>d</sup>OP + EX rats,  $P < 0.001$ . **C:** a run to exhaustion test in OP + EX and OP + COEX rats after the 10-wk diet-induced obesity study. Data are presented as individual data points ( $n = 8$ –10 animals/group) with means  $\pm$  SD bars.